# ALMA CO(2-1) observations in the XUV disk of M83

Isadora C. Bicalho, Francoise Combes, Monica Rubio, Celia Verdugo, Philippe Salome

**Astronomy & Astrophysics**

# ALMA CO(2-1) observations in the XUV disk of M83

Isadora C. Bicalho[1], Francoise Combes[1,2], Monica Rubio[3], Celia Verdugo[4], and Philippe Salome[1]

[1] Observatoire de Paris, LERMA, CNRS, PSL Univ., UPMC, Sorbonne Univ., 75014 Paris, France
e-mail: isadora.bicalho@gmail.com
[2] College de France, 11 Place Marcelin Berthelot, 75005 Paris, France
e-mail: francoise.combes@obspm.fr
[3] Departamento de Astronomía, Universidad de Chile, Chile
e-mail: mrubio@das.uchile.cl
[4] Joint ALMA Observatory, Santiago, Chile

## ABSTRACT

The extended ultraviolet (XUV) disk galaxies are some of the most interesting objects studied in the last few years. The UV emission, revealed by GALEX, extends well beyond the optical disk after the drop in H$\alpha$ emission, the usual tracer of star formation. This shows that sporadic star formation can occur in a large fraction of the HI disk at radii up to 3 or 4 times the optical radius. In most galaxies, these regions are poor in stars and are dominated by under-recycled gas; they therefore bear some similarity to the early stages of spiral galaxies and high-redshift galaxies. One remarkable example is M83, a nearby galaxy with an extended UV disk reaching 2 times the optical radius. It offers the opportunity to search for molecular gas and to characterize the star formation in outer disk regions, traced by the UV emission. We obtained CO(2-1) observations with ALMA of a small region in a $1.5' \times 3'$ rectangle located at $r_{\rm gal} = 7.85'$ over a bright UV region of M83. There is no CO detection, in spite of the abundance of HI gas, and the presence of young stars traced by their HII regions. Our spatial resolution (17 pc $\times$ 13 pc) was perfectly fitted to detect giant molecular clouds (GMC), but none were detected. The corresponding upper limits occur in a region of the Kennicutt–Schmidt diagram where dense molecular clouds are expected. Stacking our data over HI-rich regions, using the observed HI velocity, we obtain a tentative detection corresponding to a H$_2$-to-HI mass ratio of $<3 \times 10^{-2}$. A possible explanation is that the expected molecular clouds are CO-dark because of the strong UV radiation field. This field preferentially dissociates CO with respect to H$_2$, due to the small size of the star-forming clumps in the outer regions of galaxies.

**Key words.** galaxies: spiral – galaxies: ISM – galaxies: star formation – ISM: molecules – galaxies: clusters: individual: M83

## 1. Introduction

Over the last decades extended ultraviolet (XUV) disk galaxies have gained interest. Gil de Paz et al. (2005) shows the presence of UV-bright complexes in the outermost of some galaxy disks. These are called XUV disk galaxies, hosting UV emission well beyond their optical radii. UV-bright disks extending up to 3–4 times their optical radius ($R_{25}$) have been reported in about 30% of spiral galaxies (Thilker et al. 2005a; Gil de Paz et al. 2007b). Their extended UV emission covers a significant fraction of the area detected in HI at 21 cm wavelength (Bigiel et al. 2010; Boissier et al. 2003; Zaritsky & Christlein 2007). Generally, the UV star formation (SF) is related to this extending HI structure, for example showing evidence of metal enrichment (Gil de Paz et al. 2007a). Their far-ultraviolet (FUV) and near-ultraviolet (NUV) colours are generally consistent with young populations of O and B stars, which probe a wider range of ages than H$_\alpha$, and at low SF levels the number of ionizing stars may be very small (Dessauges-Zavadsky et al. 2014; Boissier et al. 2003).

Studying star formation beyond the optical radius allows us to address the condition of low-metallicity environments (Bigiel et al. 2010). The study of SF in nearby galaxies involves the star formation rate (SFR), its surface density ($\Sigma_{\rm SFR}$) and the gas surface density ($\Sigma_{\rm gas}$) including both molecular and atomic gas. The relation between these quantities is known as the Kennicutt–Schmidt (KS) relation ($\Sigma_{\rm SFR} \propto \Sigma_{\rm gas}^n$; Schmidt 1959; Kennicutt 1998; Kennicutt & Evans 2012). This relation describes how efficiently galaxies turn their gas into stars in quantifying the star formation efficiency (SFE). The KS relation is almost linear when most of the gas is molecular, providing a constant gas consumption timescale of about 3 Gyr (e.g. Bigiel et al. 2011; Saintonge et al. 2011). The SFE falls very quickly when the $\Sigma_{\rm gas} < 10\,M_\odot\,{\rm pc}^2$ when the gas is mainly atomic. However, recent surveys of molecular gas at high resolution have the sensitivity to probe this relation at $\Sigma_{\rm gas} \lesssim 3\,M_\odot\,{\rm pc}^2$. Studies of SF beyond the optical radius primarily concentrated on comparing different SF tracers. Until now studies of SFE in XUV disks were principally focused on atomic gas. These environments are not propitious to H$_2$ formation due to the low gas density and low metallicity, levels similar to galaxies in the early universe.

The confirmed occurrence of star formation in the outer disk of normal spirals has several important implications; it indicates the presence of molecular gas in the outskirts of spirals, possibly an efficient phase transition from HI to H$_2$. It is one of the regions where the unresolved issue of the atomic hydrogen gas origin can be studied: either HI is the main phase, which can be transformed to H$_2$ to form stars, or it is the product of the star formation process, i.e. the result of the photodissociation of H$_2$ by the UV flux radiation emanated from newly formed stars (Allen et al. 2004; Smith et al. 2000). It provides a simplified laboratory for

determining the star formation threshold. It is also the place where star formation can be studied in quiescent and low-metallicity environments that may affect the SFE and the initial mass function.

Crosthwaite et al. (2002) studied the overall molecular gas morphology of M83 with CO(1-0) and CO(2-1) covering the $14' \times 14'$ optical disk. In this study they found that CO falls rapidly at a radius of $5' = 7$ kpc, and they proposed that this is also the decline in the total gas surface density, even if the HI emission continues further out but with a lower surface density. Molecular gas dominates inside 7 kpc radius (80% of the gas), while in total it is only 30% of the gas. The CO(2-1)/CO(1-0) intensity ratio is ~1. At 7 kpc, where the disk begins to warp, the ISM pressure might reach a threshold for the formation of molecular clouds.

Thilker et al. (2005b) have modified this view with GALEX observations: diffuse UV emission is detected beyond the bright star-forming disk when H$\alpha$ and CO emission drop. This discovery made M83 the prototype of XUV disk galaxies. Koda et al. (2012) report deep Subaru H$\alpha$ observations of the extended ultraviolet disk of M83, and found some weak emission, not seen by Thilker et al. (2005b). Dong et al. (2008) show with *Spitzer* that the SF has been an ongoing process in the extreme outer parts of M83 for at least 1 Gyr. In a comparison between HI and FUV emission, Bigiel et al. (2010) show that the most extended atomic gas observed in M83 will not be consumed by in situ SF, and this might be due to the low efficiency of the HI-to-H$_2$ phase transition there. However, the present low SF might be sufficient for chemical enrichment. A flat oxygen abundance gradient was obtained beyond $R_{25}$ by Bresolin et al. (2009): they find only a slight decline in abundance beyond this galoctocentric distance with 12+log(O/H) between 8.2 and 8.6. Bresolin et al. (2016) present a chemical evolution model to reproduce the radial abundance gradient of M83 in $R_{25}$, and their model is able to quantify the metallicity of the gas, which is very close to that of the stars.

Star formation in low gas surface density, less than $10\, M_\odot\, \mathrm{pc}^{-2}$, is not very well known. The SFE in these regions is very low and seems to be uncorrelated with $\Sigma_{gas}$; the SFR has a much larger dynamical range than the local surface density (Boissier et al. 2007). CO observations in such environments are rare, due the weakness of the emission. A robust, quantitative picture of how the environment in the outer disks affects star formation is crucial to understanding the origins of galaxy structure. Dessauges-Zavadsky et al. (2014) were the first to study the molecular SFE in an XUV disk, M63, where they detected CO(1-0) in 2 of 12 pointings using the IRAM 30 m telescope. The authors concluded that the molecular gas in those regions has a low SFE compared to regions in the inner disk. There are only four galaxies with molecular detections in the outermost disks beyond $R_{25}$: M63 and in addition NGC 4414 (Braine & Herpin 2004), NGC 6946 (Braine et al. 2007), M33 (Gratier et al. 2010). NGC 4625 has been actively searched for CO emission, but it has not been detected (Watson et al. 2016). In these papers, the SFE is defined as $\Sigma_{SFR}/\Sigma_{H_2}$, and we adopt this definition here (Dessauges-Zavadsky et al. 2014).

In this paper, we present ALMA CO(2-1) data covering one region outside the optical disk of M83. We describe our ALMA observations in greater detail in Sect. 2, and our results in Sect. 3. Section 4 presents the discussion of the SFR in low-density and low-metallicity environments and physical reasons to explain the lack of CO emission in the outer M83 disk.

**Table 1.** M83 observations.

|  | Values |
|---|---|
| RA (centre) | $13^h 37^m 03.6^s$ |
| Dec (centre) | $-29^d 59' 47.6''$ |
| Distance (Mpc) | 4.8 |
| $R_{observed}$ | $7.85' = 11$ kpc |
| Synthesized beam | $0.75'' \times 0.56'' = 17 \times 13$ pc |

## 2. Observations

We observed CO(2-1) emission at 229.67 GHz (band 6) in M83 with ALMA during Cycle 2 (PI: Monica Rubio). The selected region is located at $13^h37^m03.6^s - 29^d59'47.6''$ enclosed in a $3' \times 1.5'$ (4 kpc $\times$ 2 kpc) rectangle located at $r_{gal} = 7.85' = 11$ kpc from M83 centre. We used the selection criteria corresponding to FUV/NUV GALEX images (Gil de Paz et al. 2007a), using the peaks of UV emission, as well as the correlation with the HI emission from the THINGS survey (Walter et al. 2008). By choosing these peaks of emission we focused on the outer parts of the UV disks, beyond the $r_{25}$ optical radius, where we are interested in detecting the molecular gas (see Fig. 1).

These selection criteria were used for the M63 XUV disk (NGC 5055), and led to a CO detection (Dessauges-Zavadsky et al. 2014) far outside the $r_{25}$ limit, while Schruba et al. (2011) only obtained an upper limit at $300''$ from the galactic centre. The selected region of M83 was observed for ~1 h in March 2014 in very good weather conditions (pwv 1.3 mm). The 12 m array was used with 34 antennas and a maximum baseline of 558.2 m. The map was prepared with a mosaic of 121 pointings separated by $12.9''$ (Fig. 2), and with an integration time of 10.8 s per pointing.

The data were calibrated using the CASA reduction package. Approximately 36% of the data were flagged, which was current at this epoch for 12 m Array data. We produced a CO(2-1) data cube for each pointing with natural weighting, and for a velocity range from 15 to 1015 km s$^{-1}$, a channel spacing of 2.5 km s$^{-1}$, and an rms of 10.3 mJy per channel. The calibrated 121 uv-tables were subsequently exported to GILDAS where the cleaning and the cube analysis were performed.

There is no continuum detection, except one weak (<2 mJy) continuum (point) source, most probably a background source, at RA = $13^h37^m00.79^s$, Dec = $-30^d00'10.8''$. Using natural weighting the synthesized beamsize of the continuum map was $0.78'' \times 0.60''$, with rms = 0.19 mJy.

For the CO line we can estimate the upper limits found in each beam, assuming a profile width of 15 km s$^{-1}$ FWHM. The rms noise level is 4 mJy in 15 km s$^{-1}$ channels for each beam of $0.75'' \times 0.56''$. The $3\sigma$ upper limit of the integrated emission is therefore 0.180 Jy km s$^{-1}$. This corresponds to L'$CO(2-1) = 2.5 \times 10^3$ K km s$^{-1}$ pc$^2$. Assuming an intensity ratio of $I_{21}/I_{10}$ 0.7 (e.g. Braine & Combes 1992), and a standard CO-to-H$_2$ conversion factor $\alpha = 4.36\, M_\odot/($K km s$^{-1}$ pc$^2$), this corresponds to $M(H_2) = 1.5 \times 10^4\, M_\odot$. This mass scale is much lower than a giant molecular cloud (GMC) in the beam of $17 \times 13$ pc.

Another way to interpret this limit is to consider that our 10.3 mJy beam$^{-1}$ noise level in 2.5 km s$^{-1}$ channels corresponds to a brightness temperature of 0.55 K. Therefore, clouds of 1.6 K should have been detected at $3\sigma$. In the outer parts of the Milky Way, as far as $R = 20$ kpc from the Galactic centre, molecular clouds up to 10 K (in CO(1-0)) and 5 K (in CO(2-1)) have been observed at similar widths
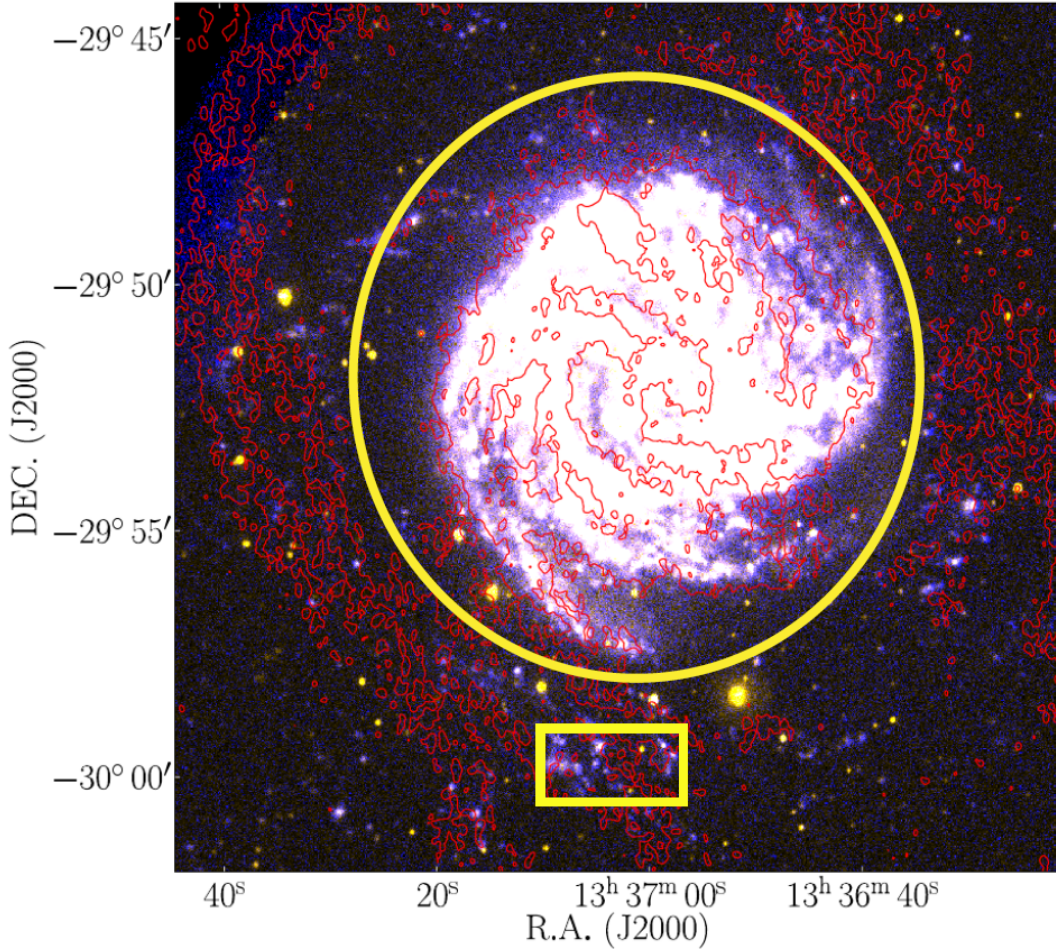
**Fig. 1.** GALEX FUV image (background) of M83 with HI contours (red). The HI emission is from the THINGS survey. The yellow ellipse shows the optical radius ($r_{25} = 6.09' = 8.64$ kpc) and the rectangle indicates the region observed with ALMA and analysed in this paper, located at $r_{gal} = 7.85' = 11$ kpc.

(e.g. Digel et al. 1994; Sun et al. 2015, 2017). They would have been detected quite easily in our survey.

## 3. Results

We searched in an automatic way for CO (2-1) emission with a S/N of more than $5\sigma$ in each of the 121 cubes, with the "detection assessment" procedure in GILDAS. We found 14 possibilities of emission, falling in the HI range of velocities (500–700 km s$^{-1}$) in this region of the galaxy, out of the 121 cubes. However, there is no spatial coincidence between these hints of emission and any of the other tracers. Also, the width of the profiles are in general too large. Therefore, evidence for the CO emission from molecular clouds is very weak.

In contrast, we look for the most prominent clumps from other tracers, in particular H$\alpha$. Using the observations from the Subaru telescope (Koda et al. 2012) we found 13 regions of star formation, and tried to search for CO emission there. These regions are shown in Fig. 3, where the circles show the spatial regions corresponding to our choice. After looking at the ALMA data, none of the hints found have more than a $3\sigma$ signal.

### 3.1. Matched filter technique

The reliable detection of weak signals is an issue in astronomical data. The data analysis process can lead us to underestimate

the probability of false detection, which is why it is necessary to estimate it. A technique that is expected to have among the best probabilities of true detection is the matched filter (MF) technique. The goal of the filter is to maximize the detectability of the signal of a known structure inside a random noise Gaussian (Vio & Andreani 2016). To better comprehend the quality of our observations (e.g. to find out whether our measurements are biased) we first apply a simple technique. Here we want to check the assumption that the probability density function (PDF) of the noise peaks is close to a Gaussian. In Vio & Andreani (2016), they show from a zero-mean map that when the positions and number of sources are unknown the matched filter might underestimate the probability of false detections. We use here the simplest technique: we plotted the pixel values from our moment 0 data. The values are plotted in Fig. 4. The plot shows no obvious irregularity or departure from a Gaussian, revealing no problem with the cleaning or reduction. Since we know that the signal should correlate to the other ISM tracer, the HI-21 cm emission, which gives us the spectral region to find the line, we apply this filter to the data through a stacking technique (see following section).

### 3.2. Stacking of CO spectra, according to the HI velocity

The CO emission is normally associated with HI peaks because the host molecular clouds probably form in regions of relatively
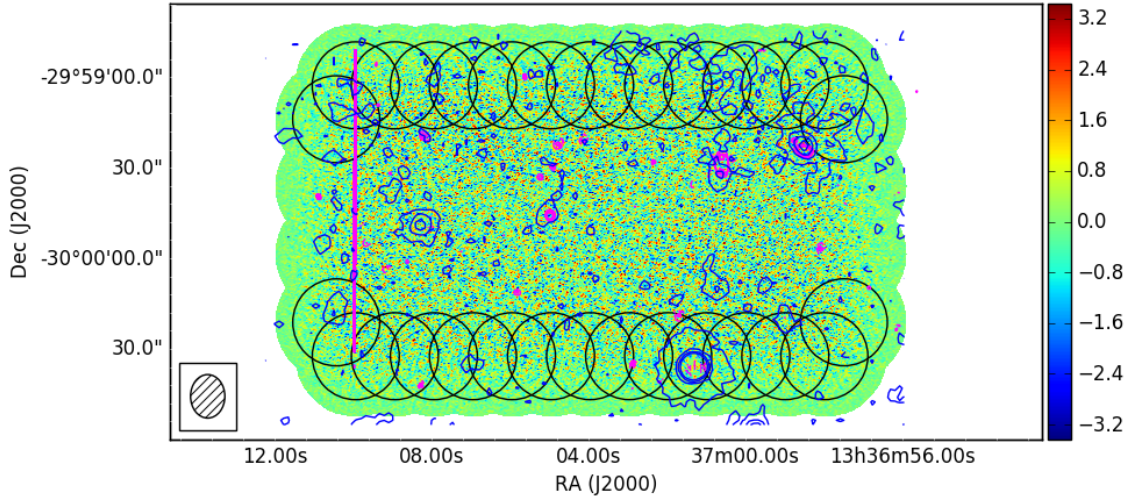
**Fig. 2.** Scheme of the ALMA mosaic of our observations. The black circles of 27″ diameter show the positions of the 121 pointings used to map the CO(2-1) emission. The background image is the CO integrated emission (zero moment of the data cube). The contours are Hα (magenta) and FIR 24 μm (black).



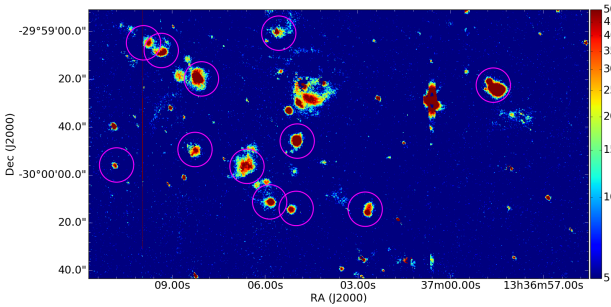**Fig. 3.** H$_\alpha$ image of the region from Subaru (Koda et al. 2012). The magenta circles show the positions where CO was searched.
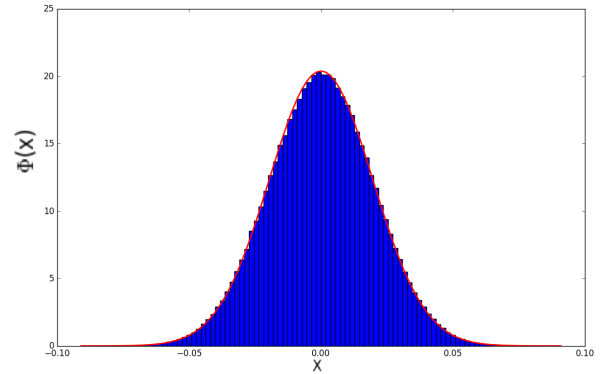


**Fig. 4.** Histogram of the pixel values from the ALMA data cube (our observations). The blue histogram comes from the pixel values and the red curve is a Gaussian fit. We see that the noise is a perfect Gaussian which does not show any indication of bumps that could be related to the reduction and deconvolution procedures.

high HI column density in the absence of spiral density waves (Gardan et al. 2007). Therefore, to exploit the full mosaic of data from ALMA, we must stack all individual spectra where emission is expected at the HI expected velocity. Averaging all pixels of the map has not given any signal; this might be due to velocity dilution since there is a significant velocity gradient of $\sim$100 km s$^{-1}$ over the corresponding HI map (see Fig. 5, right). For this CO averaged spectrum, we find an rms of 0.017 mJy in 14 km s$^{-1}$ channels. We therefore computed the first moment of the HI cube to have an average velocity at each 1.5″ × 1.5″ pixel of the map. We smoothed the CO(2-1) map at the 1.5″ resolution, and for each beam we shifted the spectra of the right velocity amount to have all of them centred at the expected velocity known from the HI spectrum. Then we averaged all spectra where the HI integrated intensity was above a certain threshold, which was 50 mJy beam × km s$^{-1}$. The same stacking was done on the HI cube, which gives the result plotted in Fig. 5, left. The resulting HI stacked spectrum has a FWHM of 33 km s$^{-1}$. No baseline was subtracted from the stacked spectra. The stacked CO(2-1) spectrum shows a hint of emission (at 3.5σ) with a FWHM of 14 km s$^{-1}$. When properly reduced, the average integrated flux is 0.85 mJy km s$^{-1}$. Adopting the conversion factor described in Sect. 2, this low value corresponds to an average mass of 65 $M_\odot$ of molecular gas per beam, but spread over $3 \times 10^4$ beams; therefore, it would represent a total mass of $2 \times 10^6$ $M_\odot$ over the whole mapped region of 4 × 2 kpc.

The same computation can be done on the averaged stacked HI spectrum. With a flux of 0.1 Jy beam km s$^{-1}$, and a beam of 15.2″ × 11.4″, this gives a total HI mass of $7.0 \times 10^7$ $M_\odot$ over the same region. The mass ratio of the molecular to the atomic gas is then $M(H_2)/M(HI) = 3 \times 10^{-2}$ or lower.

It is important to note that the stacking technique is not used here to smooth out possible extended signal on scales that would in any case be filtered out by the interferometer. On the contrary, here we aim to conserve our spatial resolution of 17 pc × 13 pc fitted to GMC scale in order to avoid dilution of the cloud emission. The stacking, as usual, averages out several realizations of possible cloud emission.

## 4. Discussion

The extended ultraviolet disks, present in 10% of nearby galaxies, offer the opportunity to study the interstellar medium and star formation in extreme conditions with low average gas density and surprisingly abundant star formation. M83 was one of the first XUV detections in its outer regions and it is the prototype for this type of galaxy. However, no highly significant
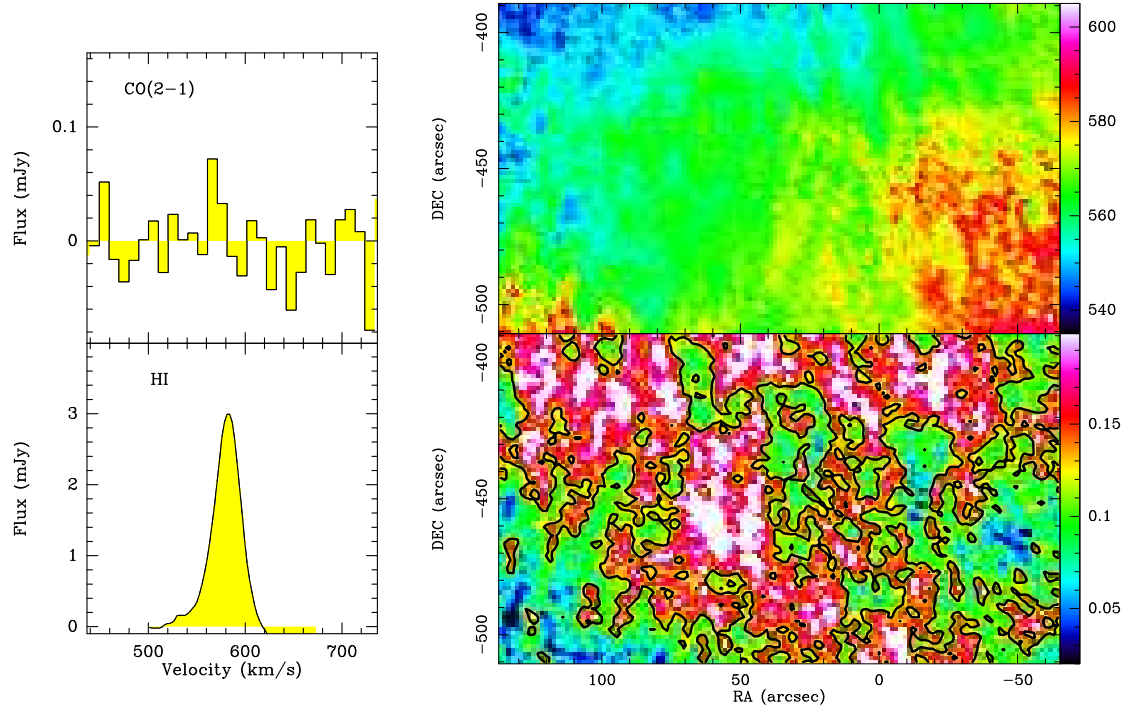
**Fig. 5.** *Left panels*: result of the stacking procedure for the CO(2-1) map (*top*) and the HI map (*bottom*). Only spectra with a significant HI detection have been considered (see text), and they have all been shifted to 580 km s$^{-1}$ central velocity. *Right panels*: HI (THINGS) integrated intensity map (Jy × km s$^{-1}$, *bottom*) in the region of the mosaic observed by ALMA, and the corresponding average velocity (*top*) in km s$^{-1}$. The spatial coordinates are in arcsec offset from the galaxy centre (13$^h$37$^m$00.9$^s$, $-$29°51′56″). The HI beam is 15.2″ × 11.4″ (VLA NA map from THINGS). The black contour corresponds to NHI = 10$^{21}$ cm$^{-2}$.

CO emission was detected in Cycle 2 ALMA maps. To analyse the impact of our observations in the context of star formation in outer XUV disks, we have investigated the behaviour in the Kennicutt-Schmidt diagram of the tentative CO detections, in plotting the equivalent molecular gas surface density, and in star formation surface density.

### 4.1. Star formation diagram

The SFR surface density can be determined from a combination of FUV and 24 $\mu$m fluxes on timescales of 10–100 Myr, using the calibration from (Leroy et al. 2008):

$$\Sigma_{SFR}(M_\odot \text{ yr}^{-1} \text{ kpc}^{-2}) = 8.1 \times 10^{-2} F_{FUV} \text{ (MJy sr}^{-1})$$
$$+ 3.2 \times 10^{-3} F_{24\mu m} \text{ (MJy sr}^{-1}) \quad (1)$$

Within an extended HII region, the very recent SFR (on a 3–10 Myr timescale) can be determined from the H$\alpha$ luminosity by (Kennicutt & Evans 2012)

$$\text{SFR}(M_\odot \text{ yr}^{-1}) = 5.37 \times 10^{-42} L(H\alpha)(\text{erg s}^{-1}) \quad (2)$$

The H$\alpha$ luminosity was corrected for internal extinction, through $L(H\alpha)_{corr} = L(H\alpha)_{obs} + 0.020L(24\mu m)$, according to Kennicutt & Evans (2012). Over an aperture of 200 pc in size around the two strongest HII regions, we find an SFR of $3 \times 10^{-4}$ and $3.6 \times 10^{-4} M_\odot \text{ yr}^{-1}$. These values are comparable to that obtained from Eq. (1). The upper limits of CO emission are also averaged over the same area (200 pc in size) to compute the corresponding surface densities. Schruba et al. (2010) have studied the dependence of the molecular depletion time in M33 on the scale considered, and they conclude that ~300 pc is the limiting scale below which the SF law as a function of gas surface density

is likely to break. We consider a very similar scale where the SF law should be relevant. We calculated the molecular hydrogen surface density as

$$\Sigma_{H_2}(M_\odot \text{ pc}^{-2}) = 4.2 I_{1-0}(\text{K km s}^{-1}), \quad (3)$$

where $I_{1-0}$ is the CO(1-0) line intensity in K km s$^{-1}$, and we assume that the CO(2-1)-to-CO(1-0) intensity ratio is $R_{21} = I_{21}/I_{10} = 0.7$. With the spatial resolution of our observations, the flux scale is 0.018 Jy K$^{-1}$. The standard CO-to-H$_2$ conversion ratio of $X_{CO} = 2 \times 10^{20}$ cm$^{-2}$/(K km s$^{-1}$) is adopted, and the number in Eq. (3) includes helium correction.

We plot the Kennicutt–Schmidt relation in Fig. 6, where we compare all the molecular data obtained in outer disks to date, with the large sample of nearby galaxies from Bigiel et al. (2008). The total gas surface density $\Sigma_{H_2} + \Sigma_{HI}$ is completely dominated by molecular gas above 9 $M_\odot$ pc$^2$, and the SFR relation can then be considered as linear with the gas surface density.

For M83, the regions used for this plot are the most prominent star-forming regions in the H$\alpha$ map. We smoothed the molecular gas surface density over the extent of the H$\alpha$ region size, about 200 pc, which leads to lower upper limits. In these regions, the average SFR surface density is high enough that we expect to find only molecular gas. We then plotted only the upper limit on H$_2$ surface density obtained by averaging over the 200 pc region. For all other compared galaxies, only the molecular component was taken into account. It can be seen that the time to consume the molecular gas in the outer regions of M83 is less ($t_{dep} < 3 \times 10^8$ yr) than the depletion time in nearby galaxies ($t_{dep} = 3 \times 10^9$ yr). It is not relevant to represent in this diagram the average value obtained through the stacking over the whole region of 4 kpc × 2 kpc since the surface densities are then diluted to a region much larger than the usual star-forming
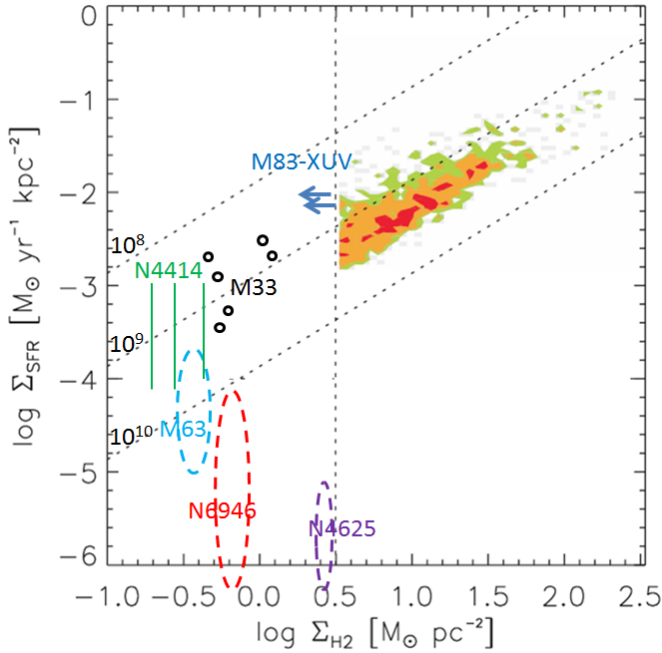
**Fig. 6.** Kennicutt–Schmidt diagram relating the SFR surface density to the molecular gas surface density, adapted from Verdugo et al. (2015) and Bigiel et al. (2008). Dashed ovals represent the data from the outer parts of XUV disk galaxies: NGC4625 and NGC6946 from Watson et al. (2016), and M63 (NGC 5055) from Dessauges-Zavadsky et al. (2014), taking only the molecular gas into account in all of them. The three green vertical bars are from NGC 4414 (Braine & Herpin 2004), and the black circles for M33 (Gratier et al. 2010). The dashed vertical line corresponds to $3\,M_\odot\,\mathrm{pc}^2$, the sensitivity limit of the CO data in Bigiel et al. (2008). Dashed inclined lines correspond to depletion times of $10^8$, $10^9$, and $10^{10}$ years to consume all the gas at the present SFR. The horizontal upper limits correspond to our CO(2-1) results on the M83 XUV disk of $\Sigma_{H_2}$, in two of the main SFR regions, 200 pc in size.

regions, used in this diagram (about 200–500 pc in size). It is indeed on such scales that a star-forming region can be defined. At lower scales, the star formation tracers, such as H$\alpha$ or FUV, are not expected to be correlated to the molecular clouds of their birth since newly born stars progressively drift away at a different velocity than the dissipative gas. For the other galaxies, the gas and SFR surface densities are also on such scales, for example M63 (Dessauges-Zavadsky et al. 2014) corresponding to the IRAM 30 m telescope beam of 0.5 and 1 kpc in CO(2-1) and CO(1-0), respectively.

### 4.2. Lack of CO emission in the outer disk of M83

One main issue in trying to explain the absence of CO emission in galaxies is the metallicity Z of the gas. It is now well established that CO emission is frequently very faint or non-existent in low-metallicity galaxies, for example in gas-rich irregular galaxies (Elmegreen et al. 1980; Tacconi & Young 1987; Taylor et al. 1998). Observations and theory both indicate that the CO to H$_2$ conversion factor, $X_{CO}$, increases at low metallicity below $12 + \log(O/H) = 8.2-8.4$ (Bolatto et al. 2013). The dependence of this relation is non-linear with Z, and may be in $Z^{-2}$ or steeper at low Z because of UV photo-dissociation in the absence of dust in addition to the underabundance of CO.

However, in the M83 field observed with ALMA, there is only a slight abundance deficiency; the average metallicity of

the H$_{II}$ regions is $12 + \log(O/H) = 8.4$ (Bresolin et al. 2009), i.e. 1/2 solar. With a slight change in $X_{CO}$ for a higher value than standard, we should still be able to detect molecular clouds at more than $8\sigma$. This means that the scatter in the $X_{CO}$–metallicity relation cannot explain the lack of CO emission.

The formation of the CO molecule occurs from OH via ion-neutral reactions that form HCO+, which after its dissociation forms CO. Thus, the CO formation rate depends on the abundance of OH, itself related to the rate of destruction by UV photons. The destruction of the CO molecule is mainly by photodissociation. In diffuse environments, the molecular clouds are more isolated, and less shielded. A schematic view of a molecular cloud includes a dense core, with CO emission, and a surface where CO is photodissociated, and emitting essentially in C+ and C lines (see Fig. 8 in Bolatto et al. 2013). Because H$_2$ and CO have similar dissociation processes in their line-transitions, H$_2$ can partially shield the CO molecule, but with large CO column densities, the CO molecule is self-shielding. At low CO column densities, and in particular in the outer parts of molecular clouds, the CO molecule is absent, and the CO-to-H$_2$ abundance ratio drops. All the carbon is found in C and C+, and this gas is called CO-dark molecular gas.

Another possible scenario which could explain the lack of CO emission is that the photo-dissociated region is fragmented into smaller clouds. Each one does not have enough depth to have CO emission, and is dominated by C+ emission. In outer disks, the small star-forming clouds will emit much less together for the same amount of gas than the larger clouds present within the optical disk. The same scenario has been invoked by Lamarche et al. (2017), who failed to detect CO emission towards the starbursting radio source 3C368 at $z = 1.13$ using ALMA data. They discuss the possibility that they observed the far-infrared fine-structure oxygen lines in star-forming gas clouds before they had the chance to form an appreciable amount of CO.

Watson et al. (2016) did not have a precise reason for not detecting CO in a young star-forming region of NGC4625, while Braine et al. (2007), Braine & Herpin (2004), and Dessauges-Zavadsky et al. (2014) were able to detect weak CO emission in the outer parts of NGC 6946, NGC 4414, and M63, respectively. However, in M63 CO is detected only in 2 out of 12 XUV disk regions. Watson et al. (2016) conclude that, even if one explanation for the lack of CO emission in lower-mass galaxies can still be the low metallicity, the issue remains for the outskirts of massive galaxies. Deeper observations are needed to disentangle the various proposed scenarios.

The gas metallicity is only half solar in our mapped ALMA field, which could already reduce the size of the CO clouds with respect to H$_2$ clouds. The lack of CO emission could also come from the excessive local FUV radiation field, which dissociates CO preferentially, and from the small size of the clouds in the outer regions of some galaxies. M83 shows particularly strong FUV emission in its outer regions with respect to others galaxies: the FUV flux ranges between 0.2 and $1.2 \times 10^{-2}$ MJy sr$^{-1}$ over our region. The resolution of the FUV observations is 100 pc at the distance of M83, so we cannot know exactly how much radiation is felt by each cloud. Although the FUV flux is much smaller than in the inner galaxy disk, clouds are smaller and less numerous in the outer parts of galaxies (here at half metallicity), which explains the more extended CO dissociation. This could be explored further through follow-up observations of the dust continuum in the Rayleigh–Jeans domain in the same region, another independent tracer of the molecular gas.

## 5. Conclusions

We have reported on a mosaic of CO(2-1) observations obtained with ALMA in the M83 outer disk, rich in atomic gas and UV emission. M83 is the prototype of spiral galaxies with an extended XUV disk.

Our aims were to map CO emission in a small region $r_{gal} = 11$ kpc from the galaxy centre. The result is a lack of CO emission, leading to the following conclusions:

1. An automatic search of CO emission in the data cube provides tentative detections of 14 clouds, but the CO(2-1) signal at 4–5$\sigma$ does not correspond spatially and spectrally to any other tracer. They are therefore considered false detections.

2. Conversely, we searched the CO map and extract the spectra at the peak of the star formation regions traced by H$\alpha$. This did not provide any CO detection higher than 3$\sigma$.

3. We stacked all the CO pixels at the places where significant HI signal is found, shifting their velocity scale to a common central velocity expected from the HI signal. This gives a hint of a detection with a profile width of $\Delta V = 14$ km s$^{-1}$. The corresponding H$_2$ mass all over the $4 \times 2$ kpc area is only $2 \times 10^6 \, M_\odot$. The H$_2$-to-HI mass ratio over this region is $<3 \times 10^{-2}$.

4. We display the CO upper limits towards the star-forming regions in the Kennicutt-Schmidt diagram, and the depletion time needed to consume the molecular gas is lower ($<3 \times 10^8$ yr) than in normal galaxy disks ($3 \times 10^9$ yr). We expected to find in some pixels of $17 \times 13$ pc GMC masses of $10^6 \, M_\odot$, while the 3$\sigma$ upper limits are $\sim 10^4 \, M_\odot$.

5. This lack of CO emission could be due partly to low metallicity since the gas abundance in this region of M83 is half solar. The average metallicity of the H$_{II}$ regions is $12 + \log(O/H) = 8.4$ (Bresolin et al. 2009). Other causes of the lack in CO may be the strong UV field, and low global density of gas and dust; the gas is predominantly H$_2$ but most carbon is not in CO molecules. In the photodissociation regions, the carbon is in C and C+.

6. In the outer parts of galaxies, at low gas surface density, the clouds are likely to be smaller than in the disk, and less self-shielded. The CO column density in each cloud is then not sufficient to avoid dissociation, and the region is dominated by C+ emission.

## References

Allen, R. J., Heaton, H. I., & Kaufman, M. J. 2004, ApJ, 608, 314
Bigiel, F., Leroy, A., Walter, F., et al. 2008, AJ, 136, 2846
Bigiel, F., Leroy, A., Walter, F., et al. 2010, AJ, 140, 1194
Bigiel, F., Leroy, A. K., Walter, F., et al. 2011, ApJ, 730, L13
Boissier, S., Prantzos, N., Boselli, A., & Gavazzi, G. 2003, MNRAS, 346, 1215
Boissier, S., Gil de Paz, A., Boselli, A., et al. 2007, ApJS, 173, 524
Bolatto, A. D., Wolfire, M., & Leroy, A. K. 2013, ARA&A, 51, 207
Braine, J., & Combes, F. 1992, A&A, 264, 433
Braine, J., & Herpin, F. 2004, Nature, 432, 369
Braine, J., Ferguson, A. M. N., Bertoldi, F., & Wilson, C. D. 2007, ApJ, 669, L73
Bresolin, F., Ryan-Weber, E., Kennicutt, R. C., & Goddard, Q. 2009, ApJ, 695, 580
Bresolin, F., Kudritzki, R.-P., Urbaneja, M. A., et al. 2016, ApJ, 830, 64
Crosthwaite, L. P., Turner, J. L., Buchholz, L., Ho, P. T. P., & Martin, R. N. 2002, AJ, 123, 1892
Dessauges-Zavadsky, M., Verdugo, C., Combes, F., & Pfenniger, D. 2014, A&A, 566, A147
Digel, S., de Geus, E., & Thaddeus, P. 1994, ApJ, 422, 92
Dong, H., Calzetti, D., Regan, M., et al. 2008, AJ, 136, 479
Elmegreen, B. G., Morris, M., & Elmegreen, D. M. 1980, ApJ, 240, 455
Gardan, E., Braine, J., Schuster, K. F., Brouillet, N., & Sievers, A. 2007, A&A, 473, 91
Gil de Paz, A., Madore, B. F., Boissier, S., et al. 2005, ApJ, 627, L29
Gil de Paz, A., Boissier, S., Madore, B. F., et al. 2007a, ApJS, 173, 185
Gil de Paz, A., Madore, B. F., Boissier, S., et al. 2007b, ApJ, 661, 115
Gratier, P., Braine, J., Rodriguez-Fernandez, N. J., et al. 2010, A&A, 522, A3
Kennicutt, Jr., R. C. 1998, ApJ, 498, 541
Kennicutt, R. C., & Evans, N. J. 2012, ARA&A, 50, 531
Koda, J., Yagi, M., Boissier, S., et al. 2012, ApJ, 749, 20
Lamarche, C., Stacey, G., Brisbin, D., et al. 2017, ApJ, 836, 123
Leroy, A. K., Walter, F., Brinks, E., et al. 2008, AJ, 136, 2782
Saintonge, A., Kauffmann, G., Wang, J., et al. 2011, MNRAS, 415, 61
Schmidt, M. 1959, ApJ, 129, 243
Schruba, A., Leroy, A. K., Walter, F., et al. 2011, AJ, 142, 37
Schruba, A., Leroy, A. K., Walter, F., Sandstrom, K., & Rosolowsky, E. 2010, ApJ, 722, 1699
Smith, D. A., Allen, R. J., Bohlin, R. C., Nicholson, N., & Stecher, T. P. 2000, ApJ, 538, 608
Sun, Y., Xu, Y., Yang, J., et al. 2015, ApJ, 798, L27
Sun, Y., Su, Y., Zhang, S.-B., et al. 2017, ApJS, 230, 17
Tacconi, L. J., & Young, J. S. 1987, ApJ, 322, 681
Taylor, C. L., Kobulnicky, H. A., & Skillman, E. D. 1998, AJ, 116, 2746
Thilker, D. A., Bianchi, L., Boissier, S., et al. 2005a, ApJ, 619, L79
Thilker, D. A., Bianchi, L., Boissier, S., et al. 2005b, ApJ, 619, L79
Verdugo, C., Combes, F., Dasyra, K., Salomé, P., & Braine, J. 2015, A&A, 582, A6
Vio, R., & Andreani, P. 2016, A&A, 589, A20
Walter, F., Brinks, E., de Blok, W. J. G., et al. 2008, AJ, 136, 2563
Watson, L. C., Martini, P., Lisenfeld, U., Böker, T., & Schinnerer, E. 2016, MNRAS, 455, 1807
Zaritsky, D., & Christlein, D. 2007, AJ, 134, 135